**Article:**
Hurtado Molina, E. orcid.org/0000-0002-4322-1263 and Long, H. orcid.org/0000-0003-1673-1193 (2025) Fretting wear in raceway-ball contact under wind turbine pitch bearing operating conditions. Wear, 564-565. 205696. ISSN: 0043-1648

https://doi.org/10.1016/j.wear.2024.205696

Wear 564–565 (2025) 205696

Contents lists available at ScienceDirect

Wear

journal homepage: www.elsevier.com/locate/wear

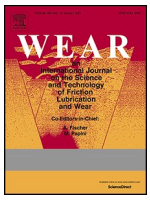

# Fretting wear in raceway-ball contact under wind turbine pitch bearing operating conditions

Eladio Hurtado Molina, Hui Long *

*Department of Mechanical Engineering, The University of Sheffield, Sheffield, S1 3JD, UK*

ARTICLE INFO

*Keywords:*
Wind turbine
Pitching bearing
Fretting
Wear
Finite element analysis

ABSTRACT

This paper investigates wear in wind turbine pitch bearings resulting from small-amplitude oscillations. The investigation focuses on assessing the impact of key parameters influencing wear damage. A new medium-scale test rig has been designed, enabling cost-efficient and accelerated tests to replicate fretting wear damage under simplified operating conditions of wind turbine pitch bearings. Through experimental result analysis, this study examines the influence of oscillation amplitude, contact force, oscillation frequency, presence of lubrication, and contact geometry on wear damage. A finite element model is also developed to obtain the frictional energy density to compare with experimentally measured wear depth to obtain new insights of the effect of the contact variables on wear damage. It has been found that most of the wear damage takes place at the location where the maximum sliding occurs but not at the location of the maximum contact pressure, while the contact geometry has an important impact on the wear damage. Controlling oscillation amplitude and contact pressure are effective ways to mitigate wear damage due to small-amplitude oscillations in wind turbine pitch bearings.

## 1. Introduction

Wear in wind turbine (WT) pitch bearings is a tribological issue that has attracted increased research interest in recent years, motivated by the challenge of improving the reliability of components in modern large-scale WTs, which are rapidly increasing their size. Pitch bearings, also known as blade bearings, connect the blades to the rotor hub of a WT. Pitch bearings allow the blades to rotate and to optimise their position under different wind speeds. Blade rotation is used to change the angle of attack of the blade to control power production and loads induced on a WT. Pitch system is also used to stop the WT operation in case of an emergency stop when an unexpected failure occurs. Therefore, accurate positioning of the blades by pitch bearings is essential to maximise productivity of WTs and to ensure their safety. A double-rowed eight-point contact ball bearing, as shown in Fig. 1, is the most widespread bearing configuration used in pitch systems of WTs.

WT pitch bearings are subjected to a combination of high axial, radial and moments loads, while standing still or oscillating at low speed to support the blades that are highly flexible components. Pitch bearings can be affected by different damage modes as described by Stammler and Reuter [1]. These damages modes can be rolling contact fatigue, core crushing, ring fractures, edge loading, false Brinelling and fretting corrosion. All these damage modes, except false Brinelling and fretting corrosion, may be assessed during the design phase of pitch bearings. False Brinelling and fretting corrosion were identified as common tribological issues of WT pitch bearings [2,3] and they had been extensively investigated. However, their similarities and differences are not clearly defined. Godfrey [4] provided one of the clearest differentiation between them: fretting corrosion is the fretting damage in unlubricated contact surfaces experiencing relative reciprocating sliding motion of small amplitudes. False Brinelling is the wear on the raceway of a lubricated rolling element bearing produced by the slight movement of the rolling elements, a condition that prevents the formation of the lubricant film. However, false Brinelling and fretting corrosion can occur simultaneously in applications depending on the operating conditions. Moreover, no clear distinction exists in literature between these two wear mechanisms, and it is still debated whether false Brinelling and fretting corrosion are different damage modes or if false Brinelling is the incubation process of fretting corrosion.

Harris et al. [2] defined fretting corrosion as a wear mode between surfaces in contact when subjected to normal load and cyclic, small-amplitude motion. These conditions squeeze lubricant out of the contact area causing direct metal-to-metal contact or boundary lubrication resulting in adhesive wear. Harris et al. [2] stated that false

* Corresponding author.
*E-mail addresses:* eladio.hurtado.m@gmail.com (E. Hurtado Molina), h.long@sheffield.ac.uk (H. Long).

https://doi.org/10.1016/j.wear.2024.205696
Received 22 July 2024; Received in revised form 24 November 2024; Accepted 6 December 2024
Available online 9 December 2024

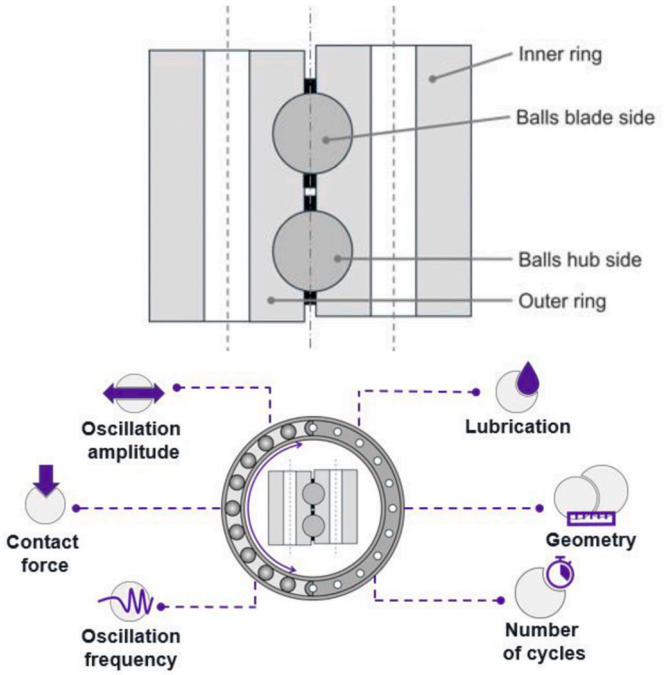


**Fig. 1.** Double-rowed eight-point contact ball bearing and key operating parameters of pitch bearing.

Brinelling was the incubation process of fretting corrosion, whereas Godfrey [4] differentiated two different wear modes based on the lubrication condition. Recent studies on false Brinelling in pitch bearings defined false Brinelling as a form of fretting wear [5,6]. In terms of the wear process, Godet [7] and Berthier et al. [8] described wear produced by reciprocating motion as a process of debris formation and ejection. The wear process can be controlled by the rate of debris formation or ejection, depending on the contact geometry. In non-conforming contacts, debris are easily ejected and the wear rate is controlled by the rate of debris formation.

Fretting is a complex wear mode that can involve different wear mechanisms, such as adhesion, abrasion, and oxidation. Regarding the oxidative wear process, Godfrey [4] observed Hematite $Fe_2O_3$ as the oxidation product of fretting corrosion and Magnetite $Fe_3O_4$ of false Brinelling. These two iron oxides have different oxidation states, which means that the formation of Hematite needs more oxygen than forming Magnetite [9]. This implies that fretting corrosion occurs in an oxygen-richer environment. However, no clear explanation has been found in published studies to understand why one oxidation product will form over the other in fretting. It has been suggested that this difference is attributed to the lubrication condition: lubricated for false Brinelling and unlubricated for fretting corrosion. However, pitch bearings are grease lubricated and they can experience both wear modes. Although lubrication plays an important role in preventing the access of oxygen into the contact area, the differentiation of these wear modes in pitch bearings is more complex than simply categorising the fretting contact as unlubricated or lubricated condition.

More than 50 parameters have been reported to be related to fretting wear [10] and they have exhibited a strong interconnection. Collins [10] suggested that these variables could be grouped into eight big categories: slip amplitude, contact pressure, local state of stress, number of cycles, material and surface conditions, cyclic frequency, temperature, and surrounding environmental conditions. When analysing fretting wear, the number of these groups could be further reduced, and relevant parameters are grouped into four categories: motion profile, load, bearing geometry and lubrication. Oscillation amplitude has been recognised as one of the most important factors associated with false Brinelling and fretting corrosion. These wear modes take place under small-amplitude oscillations; however, the range for small amplitude oscillations is not clearly defined. The sliding ratio, $x/2b$, is usually considered to define a normalised parameter, where $x$ corresponds to the oscillation amplitude and $2b$ is the width of the contact area. For classic fretting, wear is argued to occur when sliding ratios are lower than 1.0 [11]. For oscillating bearing applications, a threshold of the sliding ratio, $x/2b = 1.6$, has been defined as the minimum value to ensure the formation of lubrication film in the contact area [12]. However, in most recent research investigating fretting, wear has occurred in oscillating bearings under larger sliding ratios, up to $x/2b = 13.3$ [13]. In fact, the wear damage has been found to be more severe under larger sliding ratios.

False Brinelling and fretting corrosion are commonly investigated through experimental methods that involve the use of reduced-scale samples and standard tribometer configurations [14,15]. However, such testing approaches often overlook the complex contact conditions experienced by pitch bearings during their operation. When studying these wear modes under specific operating conditions of pitch bearings, experimental setups are also typically conducted on a small-scale [16, 17] due to the substantial cost associated with testing actual pitch bearings. This approach may inadvertently disregard the impact of scale on the results obtained. Numerical methods have also been employed for analysing the behaviour of pitch bearings. Specifically, finite element analysis (FEA) can be utilised to investigate the bearing load distribution, deformation of bearing raceway rings, and the contact parameters relevant to false Brinelling and fretting corrosion as wear modes [17–20]. However, this approach often lacks robust validation due to simplifications made when setting up the FEA models [21]. Challenges arise in accurately representing lubricated contacts and the limited information available on actual working conditions and failures of WT pitch bearings.

To describe the wear mechanisms of oscillating sliding contacts, Fouvry et al. [11] proposed an energy approach to consider the effect of variable coefficient of friction behaviour on the wear coefficient. This energy approach consists of comparing the wear volume ($V$) with the accumulated frictional energy dissipated at the contact area ($Ed$). This energy corresponds to the energy enclosed in every fretting loop cycle. Fouvry et al. [11] observed a linear relationship between the wear volume and the accumulated dissipated energy. An energy wear coefficient ($\alpha_V$) could be obtained by calculating the slope of the linear curve. For some metallic materials, the linear curve did not cross the origin of the diagram relating the wear volume and the accumulated frictional energy dissipated. The offset in the energy axis was associated with an energy threshold ($Ed_{th}$) required to modify the microstructure of the contact surface to a harder phase known as tribologically transformed structure (TTS). The fracture of the TTS was found to lead to the debris formation. The energy wear approach to determine the wear volume is then expressed by Equation (1).

$$V = \begin{cases} 0, & if \sum Ed \le Ed_{th}, \\ \alpha_V \left( \sum Ed - Ed_{th} \right), & if \sum Ed > Ed_{th} \end{cases} \quad (1)$$

Fouvry et al. [11] highlighted that the wear volume analysis was a powerful tool to quantify fretting wear but also pointed out that the wear damage was frequently assessed in one dimension, the depth of the worn surface. For this reason, a local wear analysis was needed. The local wear approach consisted of comparing the wear depth ($h$) with the dissipated energy density ($Ed_h$). Similarly to the wear volume approach, a linear relationship was observed between these two variables and a local wear coefficient ($\alpha_h$) could be derived from the slope. The energy density dissipated at a specific point of the contact surface is given by the expression of Equation (2) for an oscillation displacement of $2x$.

$$Ed_h(x,y) = \int_{-x}^{+x} q(x,y)ds \quad (2)$$

where $q(x, y)$ is the shear stress of the contact surface. The wear depth, $h$, is then expressed by Equation (3).

$$h = \alpha_h \sum Ed_h \quad (3)$$

Schwack et al. [17] conducted both finite element simulations and experimental analysis to investigate the wear caused by small-amplitude oscillations in an 80 mm diameter ball bearing. They utilised frictional work density as an indicator of the wear and validated its accuracy by comparing the distribution of frictional energy density with the damaged area observed in the experimental tested bearings.

This study investigates the impact of key parameters on fretting wear under pitch bearing operating conditions, these are outlined in Fig. 1. A new test rig capable of evaluating medium-scale ball pitch bearings has been designed and manufactured for experimental testing of balls of 25–28 mm diameter under ball-raceway contact conditions emulating those of ball pitch bearings. Furthermore, this study is enhanced through the development of wear modelling based on finite element analysis, which obtains valuable insights into the contact variables that cannot be controlled or easily measured experimentally. A number of key insights have been obtained through this study: firstly, most of the wear takes place at the location where the maximum sliding occurs but not at the location of the maximum contact pressure, which shows the greater contribution of the sliding distance to the frictional energy density; secondly, contact geometry has an important impact on the wear damage; and lastly, controlling oscillation amplitude and contact pressure can be effective ways to mitigate wear damage due to small-amplitude oscillations in WT pitch bearings.

## 2. Materials and investigation methods

### 2.1. Fretting test rig

A new fretting test rig has been designed and manufactured to replicate wear occurring in a ball-raceway contact configuration under simplified operating conditions of pitch bearings. The designed experimental setup allows the investigation of how the key testing parameters affect fretting wear, including oscillation amplitude, contact force, oscillation frequency, lubrication, contact geometry and number of cycles. The new fretting test rig has been specifically designed to be integrated into a bi-axial machine comprises four linear actuators capable of operating using both force and displacement controls under static and dynamic conditions. This setup enables, for example, the application of a constant force along one axis direction while allowing for variable displacement along the second axis direction. The relevant specifications of the bi-axial machine are presented in Table 1.

The contact configuration plays a crucial role in obtaining accurate wear marks representative to that of WT pitch bearings under small-amplitude oscillations. However, due to the linear actuators used in the bi-axial machine, certain simplifications are necessary when designing the contact geometry of the samples. The first simplification involves suppressing the curvature of the bearing rings from the samples. Considering the range of diameters typically employed in pitch bearings, between 2 and 5 m, the effect of this curvature is negligible under small-amplitude oscillations. The second simplification is related to the contact angle. In ball pitch bearings, the nominal contact angle is commonly 45° and it varies during blade pitching operation [22]. In the proposed contact configuration of the fretting test rig design, the contact angle is defined to be zero. These simplifications significantly reduce the ball spinning. However, the balls can roll over the grooved surfaces of the samples in this contact set-up when the oscillatory motion is applied to one of the samples. Fig. 2a provides a schematic comparison between the contact configuration in a pitch bearing and the proposed contact geometry in the fretting test rig design of this study.

**Table 1**
Main specifications of the bi-axial machine.

| Parameter | Value |
|---|---|
| Maximum distance between actuators [mm] | 475 |
| Minimum distance between actuators [mm] | 425 |
| Load range [kN] | 0–100 |
| Oscillation amplitude range [mm] | 0–50 |
| Oscillation frequency range [Hz] | 0–10 |

Fig. 3 shows the fretting test rig mounted on the bi-axial machine. The test rig is designed with three attachment parts that connect the rig to the top, bottom and one of the lateral actuators, as well as two sample holders. The top holder is assembled to the top attachment and the bottom holder to the lateral actuator by means of bolted connections. The bottom holder is supported by the bottom attachment where a 3 mm PTFE plate acts as a low-friction slider at the interface of these two components. The application of the contact load is achieved through the top actuator, while the lateral actuator enables the oscillatory movement. The lateral actuator allows the measurement of the tangential force. This measurement, together with the applied contact load, is used to estimate the coefficient of friction; assuming that the frictional force between the balls and the grooved surfaces are the major contributors to the tangential force measured by the lateral actuator. This assumption means that the coefficient of friction in the sliding plate is assumed considerably lower. The proposed design consists of two balls and two raceway samples. Two balls improve the stability of the experiment and effectively prevents any ball from deviating away from the force application line. Moreover, the use of two balls generates two distinct wear marks on each sample, thereby increasing the repeatability of the tests. To ensure that each ball shared an equal load from the top actuator, it is necessary to maintain a uniform distance between each ball and the force line. This is achieved by using a 3D-printed ball positioning aid.

### 2.2. Samples and lubrication

WT pitch bearings are typically manufactured using bearing steel, specifically the 42*CrMo*4 alloy steel (EN19) [23]. Raceways are induction hardened, where a surface hardness of 60 HRC is achieved. However, induction hardening is not a suitable heat treatment method for the scale of the samples being considered in the wear tests of this study because it significantly increases the cost of the samples. Therefore, through hardening has been chosen as a more cost-efficient alternative to achieve the required surface hardness. This method allows all the samples to be heat treated in the same batch. However, due to the microstructure of 42*CrMo*4 steel, it is not possible to achieve a hardness of 60 HRC by through hardening. Thus, tool steel O1 is used as an alternative material for sample production. A comparison of the chemical composition between 42*CrMo*4 and O1 steels is provided in Table 2 [23,24]. Regarding the raceway surface finish, a maximum *Ra* value of 1.642 μm is specified, which falls within the upper limit of the typical roughness range required for pitch bearings. The tests utilise AISI 52100 grade 100 balls with diameters of 25 mm and 28 mm.

Regarding lubrication, this study looks into the effect of dry and lubricated contacts. For the lubricated contact tests, a lithium complex grease, specifically Castrol LMX, has been chosen. The properties of this grease fall within the average range of values for greases commonly used in pitch bearing applications. It is important to note that the selection of this grease does not guarantee its effectiveness in reducing wear under the specific test conditions. Table 3 presents the properties of the grease used in the tests, as well as those of six other reference greases for comparison purposes [13].

### 2.3. Testing conditions

A total of 24 tests are conducted using the developed medium-scale fretting test rig. These tests consist of 12 different combinations of varied testing parameters, including oscillation amplitude, contact force, oscillation frequency, ball size, conformity and number of cycles. The

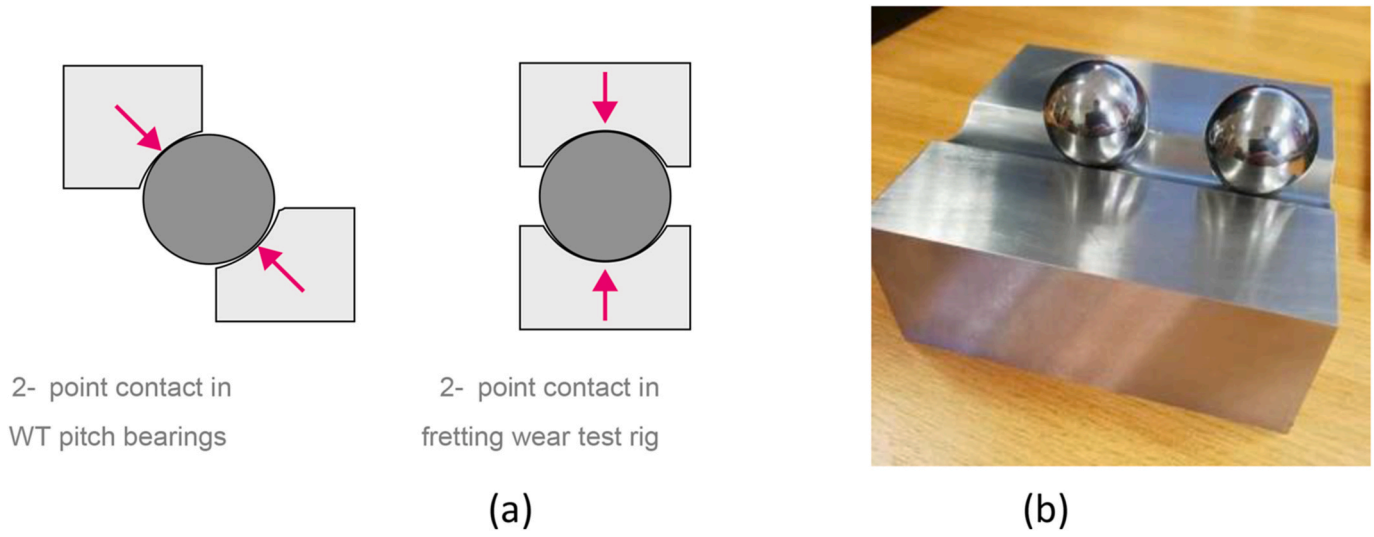


**Fig. 2.** Comparison between 2-point contact in WT ball pitch bearing: (a) the simplified contact geometry in the test rig and (b) manufactured raceway sample and balls creating grooved surface contact.

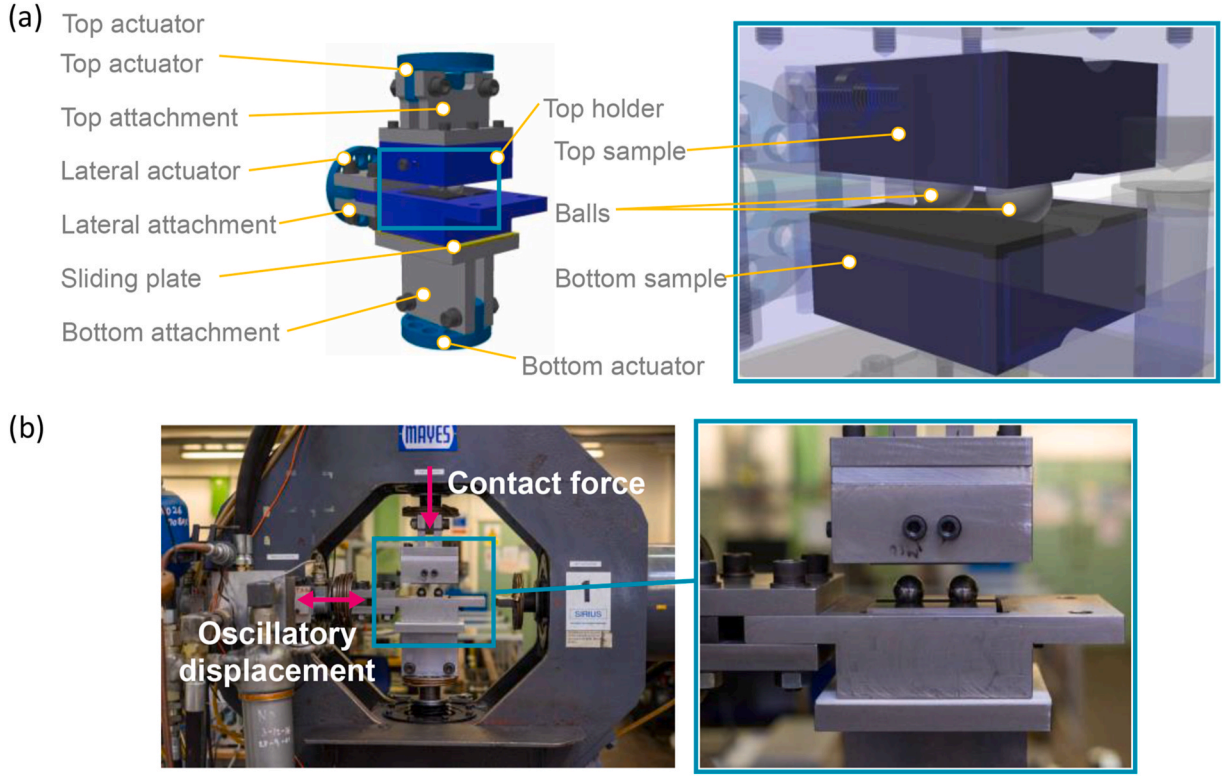


**Fig. 3.** Fretting test rig designed: (a) CAD model including interfaces to the bi-axial machine and (b) test rig mounted on the bi-axial machine.

**Table 2**
Comparison of chemical composition between $42CrMo_4$ and O1 steels.

| Element | $42CrMo_4$ | O1 |
|---|---|---|
| Carbon | 0.35–0.45 % | 0.95 % |
| Manganese | 0.50–0.80 % | 1.25 % |
| Vanadium | – | 0.20 % |
| Chromium | 0.90–1.50 % | 0.50 % |
| Tungsten | – | 0.50 % |
| Molybdenum | 0.20–0.40 % | – |
| Silicon | 0.10–0.35 % | – |

experiments are conducted under both unlubricated and grease lubricated conditions. The testing conditions for each of the 24 tests are outlined in Table 4. Additionally, Table 5 provides a summary of the maximum contact pressure, width of contact area (calculated using Hertzian contact equations), and the normalised oscillation amplitude for the various testing parameters considered in the study. The criteria to define the range of each testing parameter are described as follows.

1. **Oscillation amplitude**: Although classic fretting wear is commonly argued to occur for sliding ratios below 1.0 [11], establishing a clear limit for complex contact interfaces, such as balls in contact with

**Table 3**
Properties of selected grease and comparison with reference greases [13,25].

| Grease | Base oil | NLGI | Thickener | Base oil viscosity @40 °C |
|---|---|---|---|---|
| **Tested grease** | **Mineral** | **2** | **Lithium complex** | **180** |
| Grease 1 | Synthetic | 2 | Lithium | 50 |
| Grease 2 | Ester | 2 | Lithium | 295 |
| Grease 3 | Synthetic | 1–2 | Lithium complex | 420 |
| Grease 4 | Mineral/ Synthetic | 1–2 | Calcium | 13 |
| Grease 5 | Mineral/ Synthetic | 2 | Calcium complex | 134 |
| Grease 6 | Mineral/ Synthetic | 1 | Lithium complex | 130 |

raceways in WT pitch bearings, remains a challenge. In the specific case of pitch bearings, fretting wear has been observed when sliding ratios exceed 1.0 [13,26]. In fact, it has been found that intermediate oscillation amplitudes, resulting in a sliding ratio of approximately 10, induce severe wear damage than that by smaller oscillations where the sliding ratio is below 1.6 [13]. In this experimental study, oscillation amplitudes of 2.0 mm, 5.0 mm, 8.0 mm are tested. These values could correspond to sliding ratios ranging from 1.4 to 7.8 if the far-field displacement are equal to the actual contact sliding [27]. However, considering the presence of elastic effects on the contact surfaces, the actual sliding distance and corresponding sliding ratios are expected to be smaller.

2. **Contact force**: Fretting wear is argued to take place under high contact pressure [2]. WT Design Guideline DG03: Yaw and Pitch Rolling Bearing Life [2] recommends a maximum contact pressure of 2.4 GPa to avoid the occurrence of fretting wear under mean operating conditions. However, Schwack et al. [17] observed false Brinelling and fretting corrosion wear marks in small-scale bearings with contact pressure under 2 GPa. The contact forces in the tests of this study is designed in the range from 10 to 30 kN, resulting in the maximum contact pressure between 2.2 and 3.2 GPa.
3. **Oscillation frequency**: Small oscillations in pitch bearings take place in the range of 0.5 Hz–2 Hz [28]. The same frequency range is considered in the tests of this study.
4. **Number of cycles**: The maximum number of cycles is defined considering two criteria. Firstly, the measurement of coefficient of friction has to exhibit stable and steady behaviour. Secondly, the wear mark must be well-developed to be measurable. By conducting preliminary tests, it has been found that these two requirements are met for tests lasted for 10,000 cycles. One of the parameters combinations tested 3000 cycles to obtain insights into the temporal evolution of the wear damage.
5. **Contact geometry**: The ball diameter is 25 or 28 mm by considering the load capacity constraint of the bi-axial machine and the required contact pressures. To investigate the effect of conformity, defined as the ratio between the raceway radius and the ball diameter, change of the ball diameter and raceway radius are considered in the tests to investigate their impact on the wear damage.

### 2.4. Wear measurement

The Alicona InifiteFocus-SL is used to carry out the surface mapping of the tested surface of samples. The Alicona InifiteFocus-SL is a high-resolution non-contact optical measurement tool capable of measuring 3D surfaces to a resolution up to 10 nm. The post-processing of the

**Table 5**
Tested maximum contact pressure, half width of contact area, and normalised oscillation amplitude.

| Contact force [kN] | Max. Contact pressure [GPa] | Half contact area width b [mm] | Normalised oscillation amplitude by x/2b | | |
|---|---|---|---|---|---|
| | | | x = 2 mm | x = 5 mm | x = 8 mm |
| 10 | 2.2 | 0.51 | 1.95 | 4.88 | 7.81 |
| 20 | 2.8 | 0.65 | 1.55 | 3.88 | 6.20 |
| 30 | 3.2 | 0.74 | 1.36 | 3.39 | 5.42 |

**Table 4**
Testing conditions for unlubricated and grease lubricated conditions.

| Dry tests | | | | | | | |
|---|---|---|---|---|---|---|---|
| Test ID | Ball diam. [mm] | Raceway rad. [mm] | Conformity | Osc. Amp. [mm] | Cont. For. [kN] | Osc. Freq. [Hz] | Cycles |
| D01 | 25 | 13 | 0.52 | 5.0 | 20 | 1.0 | 10000 |
| D02 | 25 | 13 | 0.52 | 2.0 | 20 | 1.0 | 10000 |
| D03 | 25 | 13 | 0.52 | 8.0 | 20 | 1.0 | 10000 |
| D04 | 25 | 13 | 0.52 | 2.0 | 10 | 1.0 | 10000 |
| D05 | 25 | 13 | 0.52 | 5.0 | 10 | 1.0 | 10000 |
| D06 | 25 | 13 | 0.52 | 2.0 | 30 | 1.0 | 10000 |
| D07 | 25 | 13 | 0.52 | 5.0 | 30 | 1.0 | 10000 |
| D08 | 25 | 14 | 0.56 | 5.0 | 20 | 1.0 | 10000 |
| D09 | 28 | 14.56 | 0.52 | 5.0 | 20 | 1.0 | 10000 |
| D10 | 25 | 13 | 0.52 | 5.0 | 20 | 1.0 | 3000 |
| D11 | 25 | 13 | 0.52 | 5.0 | 20 | 0.5 | 10000 |
| D12 | 25 | 13 | 0.52 | 5.0 | 20 | 2.0 | 10000 |
| Lubricated Tests | | | | | | | |
| Test ID | Ball diam. [mm] | Raceway rad. [mm] | Conformity | Osc. Amp. [mm] | Cont. For. [kN] | Osc. Freq. [Hz] | Cycles |
| L01 | 25 | 13 | 0.52 | 5.0 | 20 | 1.0 | 10000 |
| L02 | 25 | 13 | 0.52 | 2.0 | 20 | 1.0 | 10000 |
| L03 | 25 | 13 | 0.52 | 8.0 | 20 | 1.0 | 10000 |
| L04 | 25 | 13 | 0.52 | 2.0 | 10 | 1.0 | 10000 |
| L05 | 25 | 13 | 0.52 | 5.0 | 10 | 1.0 | 10000 |
| L06 | 25 | 13 | 0.52 | 2.0 | 30 | 1.0 | 10000 |
| L07 | 25 | 13 | 0.52 | 5.0 | 30 | 1.0 | 10000 |
| L08 | 25 | 14 | 0.56 | 5.0 | 20 | 1.0 | 10000 |
| L09 | 28 | 14.56 | 0.52 | 5.0 | 20 | 1.0 | 10000 |
| L10 | 25 | 13 | 0.52 | 5.0 | 20 | 1.0 | 3000 |
| L11 | 25 | 13 | 0.52 | 5.0 | 20 | 0.5 | 10000 |
| L12 | 25 | 13 | 0.52 | 5.0 | 20 | 2.0 | 10000 |

measured surfaces involves straightening the measured surface by applying a *Form Removal utility*. This utility straightens the overall shape of the measured object by keeping the roughness profile of the measured surface unaffected. This makes it possible to measure the wear mark dimensions using an appropriate coordinate system. All the data is exported as text file and analysed using a Python code developed to measure the dimensions of the wear marks and plot the wear mark profiles.

### 2.5. Finite element analysis of frictional energy density

In this study, a similar approach to the one used by Schwack et al. [17] is employed, where a finite element model is developed to examine the frictional work density, as a wear indicator, using the same contact configuration as that of the fretting wear tests. The wear indicator is obtained from the FE model to compare with the measured wear depth from the experimental tests. By doing so, the model and the frictional work density can be validated as indicators of wear damage, potentially allowing for the prediction of wear damage accumulation based on Equation (3).

The FE model of this study is developed using ABAQUS EXPLICIT. The analysis aims to investigate different contact parameters, such as the contact pressure, shear stress, sliding distance and frictional energy density under the same conditions tested experimentally. One ball and two raceway sample sections are considered in the FE model. The assembly of these parts is presented in Fig. 4a. The material properties considered for the grooved samples and the ball are the steel's Young Modulus of 200 GPa and Poisson's ratio of 0.3.

All the parts of the FE model are modelled as solid bodies and meshed with eight-node fully integrated brick elements (C3D8). The raceway samples are partitioned into two regions: a region near the contact interface with the ball, where a finer mesh is defined, and the rest of the sample is meshed with coarse elements. The FE mesh developed for this model is presented in Fig. 4a. In order to ensure the numerical accuracy of the results, a mesh convergence study is conducted by evaluating the contact pressure (CPRESS) and the slip magnitude (CSLIPEQ). The error of both variables is found to be below 5 % in the refined models. These results are achieved by considering an element size of 0.15 mm in the contact region.

The interactions, boundary conditions and loads applied to this FE model are shown in Fig. 4b. Since the aim of this FE model is to study the effect of the different testing conditions, different values of the oscillation amplitude, contact force, and contact geometries are considered. The different modelling conditions evaluated by using this FE model are summarised in Table 6. Fig. 4b shows a scheme of the loading and displacement applied, which are explained as follows.

1. A reference point is created at the centre of the top face of the upper sample and linked to the surface where contact force is applied by means of a coupling constraint. The force is applied in the vertical direction (y axis) and all the other degrees of freedom of the reference point are fixed. Similarly, a reference point is also created at the centre of the bottom face of the lower sample and linked to the surface where the oscillatory motion is applied by means of a coupling constraint. The oscillatory displacement is applied in the lateral direction (z axis) and all the other remaining degrees of freedom of the reference point are fixed.
2. A contact interaction is defined between the ball and each of the grooved samples with a coefficient of friction of 0.1. This value was chosen as representative value of the coefficient of friction measured during the tests, and the detailed discussion is presented in section 3.3. The surfaces of the grooved samples are defined as master surfaces and the ball's outer face as slave surface. Coulomb's isotropic friction is defined as tangential behaviour and hard contact as the normal behaviour. The contact algorithm is set as the penalty method. The two meshing regions of each grooved sample are assembled through a tie constraint.

**Table 6**
Different conditions evaluated in the FE model.

| Model | COF | Osc. Amp [mm] | Force [kN] | Freq. [Hz] | Ball diam. [mm] | Conformity |
|---|---|---|---|---|---|---|
| 01 | 0.1 | 2 | 20 | 1 | 25 | 0.52 |
| 02 | 0.1 | 5 | 20 | 1 | 25 | 0.52 |
| 03 | 0.1 | 8 | 20 | 1 | 25 | 0.52 |
| 04 | 0.1 | 5 | 10 | 1 | 25 | 0.52 |
| 05 | 0.1 | 5 | 30 | 1 | 25 | 0.52 |
| 06 | 0.1 | 5 | 20 | 1 | 28 | 0.52 |
| 07 | 0.1 | 5 | 20 | 1 | 25 | 0.56 |

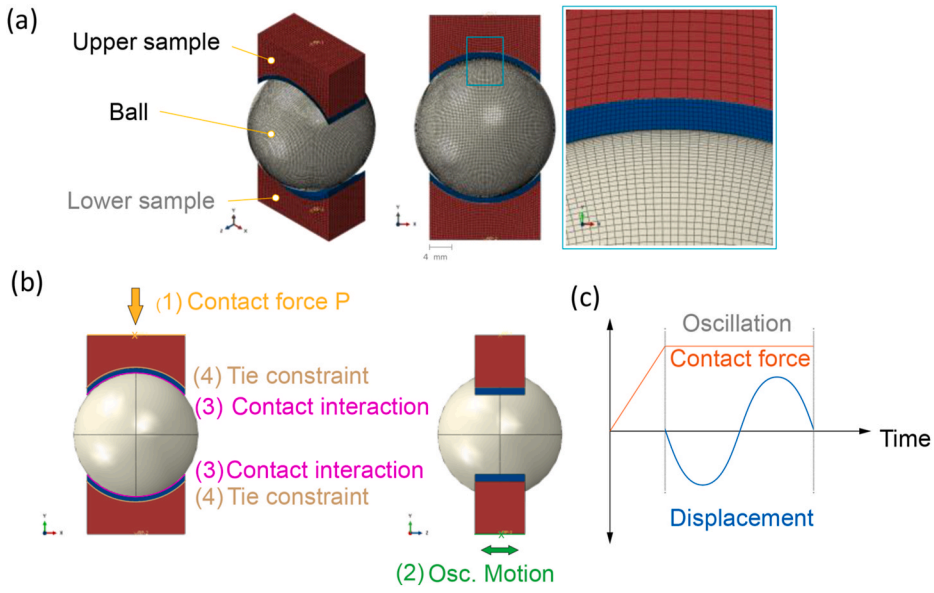


**Fig. 4.** Rolling ball on curved surface contact FE model: (a) meshes of raceways and ball; (b) Boundary conditions, interactions and loads, and (c) Loading and oscillation sequence.

## 3. Results of experimental tests and FE models

### 3.1. Characterisation of wear damage

Fig. 5 presents the wear marks using both texture and height colour maps for tests D01 and L01. These wear marks exhibit similar wear patterns consisting of three regions, A, B and C. Region A is located at both ends of the long axis of the worn area. In this region, high levels of oxidation can be observed, as well as the highest wear depth. Region B is located at the centre with lower levels of oxidation and less accumulated wear damage. Evidence of sliding of the ball that shifted the centre of oscillation is also observed, which explains the small amount of wear on the left of both wear marks, probably produced during the early cycles of the test. After these early cycles, the oscillatory movements has been stabilised at region C, where most the wear damage is concentrated. Similar patterns are observed from all samples of the conducted tests.

The highest level of oxidation is observed at the outer region of the wear marks where the contact pressure is minimum. In addition to the oxidation, the maximum sliding takes place at region A. This sliding is mainly produced by a combination of Heathcote slip [29] and elastic slip. Heathcote [29] studied microslips in closely conforming contacts of a hard ball on a grooved surface and determined that rolling without sliding was only possible along two lines of the contact area and slip was produced by the difference of surface velocities. Elastic slip is resulted from the deformation of the two surfaces in contact when loaded to establish the contact area. The elastic slip was argued to be more relevant when the two bodies had dissimilar elastic properties [30]. Equations derived by Heathcote did not take into account the elastic slip [31]. Johnson [32] considered both Heathcote and elastic slip to describe the sliding behaviour of a rolling ball on a raceway and identified that sliding or microslip took place along all the contact area length, except at the narrow bands of pure rolling. It also concluded that it was possible to have a locked region depending on the coefficient of friction.

The dimensions of the worn area of the tested sample under dry condition D01 are approximately 5 % larger than the grease lubricated worn area L01. Both worn areas are produced by the same ball in contact with top (dry) and bottom (lubricated) specimens during the same test. Therefore, the difference in dimensions of the worn area can only be attributed to the lubricant. However, the maximum wear depth are almost the same for both tests (60 μm).

To understand the effect of lubrication on the wear damage better, Fig. 6 presents the wear mark profiles along the long axis of the worn area at the location of the maximum depth (A) and at the centre of the wear mark (B). Both profiles show a w-shape. The main difference is that in the profile along the line A the wear is mostly accumulated at the end of elliptical contact area, while along the line B, the wear is mostly

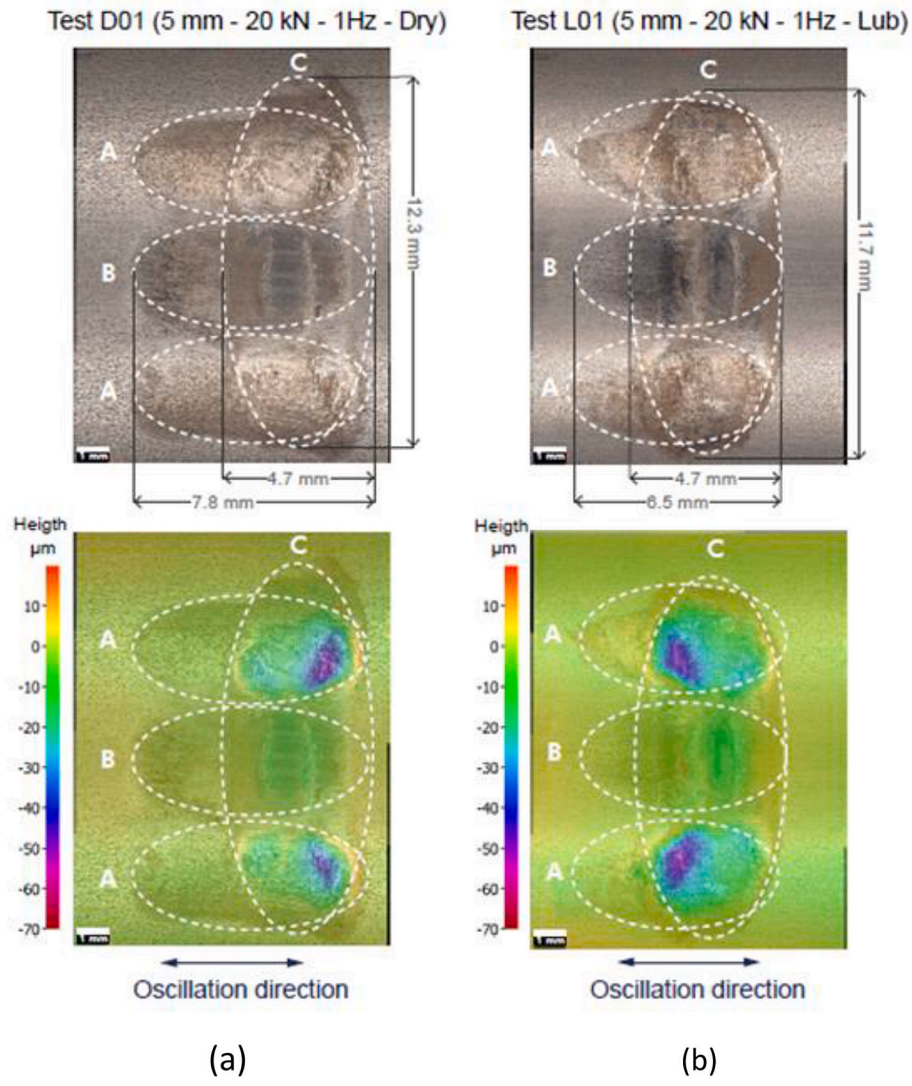


**Fig. 5.** Surface measurements of samples from tests: (a) D01 and (b) L01 using texture and height colour maps respectively. (For interpretation of the references to colour in this figure legend, the reader is referred to the Web version of this article.)

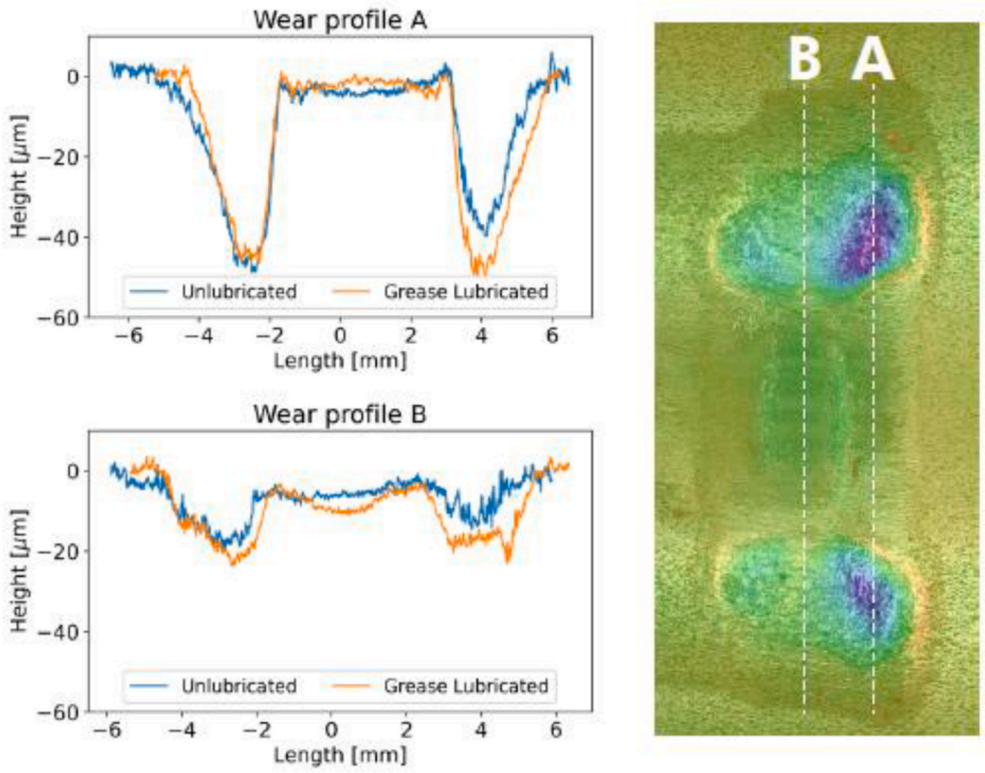


**Fig. 6.** Wear mark profiles of tests D01 and L01.

located at the zero-crossing with smaller wear observed at the centre. This difference suggests the presence of a locked region at the centre with minimal wear.

A metallographic analysis is conducted on the sample of test D01 to examine its microstructure as raw material without heat treatment, after the heat treatment, and after the test. Fig. 7a depicts the microstructure

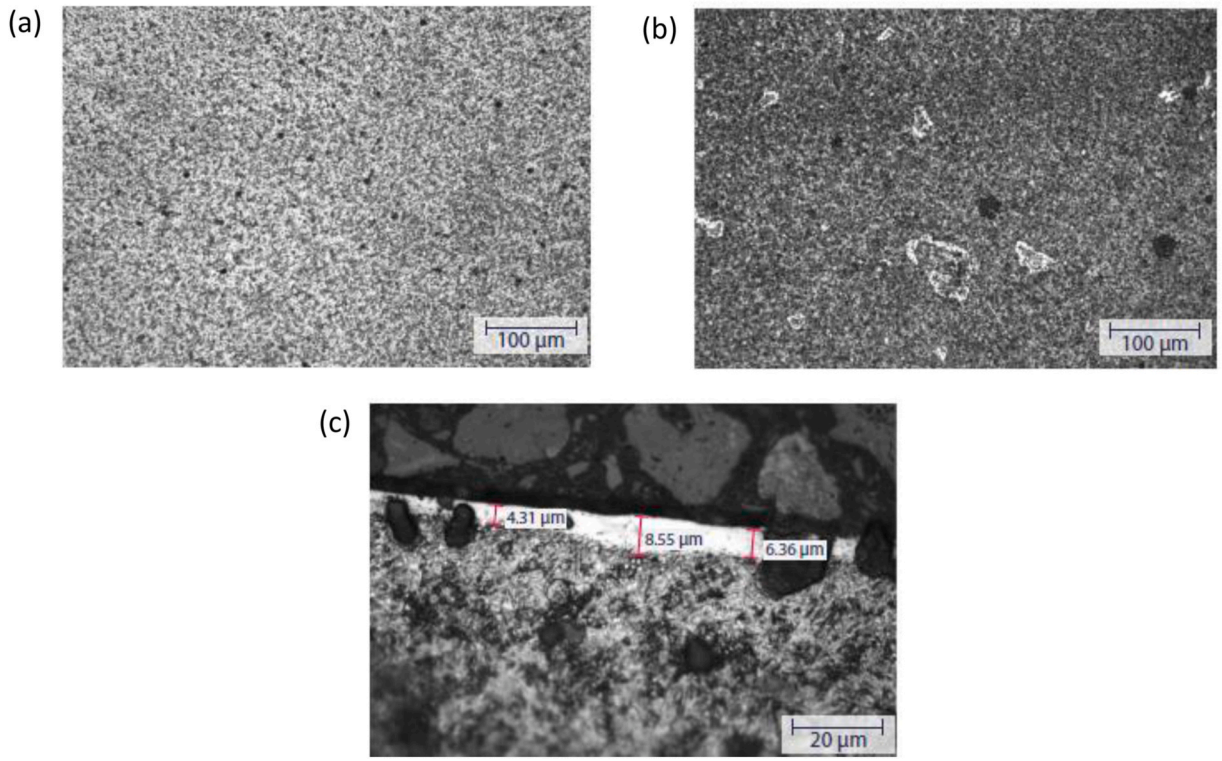


**Fig. 7.** Metallographic analysis of AISI O1 steel sample using optical microscope: (a) before heat treatment (x20), (b) after heat treatment (x20) and (c) after test (x100).

of the annealed sample corresponding to a fine microstructure of cementite or iron carbide $Fe_3C$ [33]. Fig. 7b shows the microstructure of the heat-treated sample, consisting of tempered Martensite with small carbides [33]. Fig. 7c shows the cross section of a tested sample just underneath a wear mark. The presence of a thin white layer just under the contact surface can be observed. This layer extends along the whole wear mark length and its average thickness is 6.4 ± 1.7 μm. This microstructural feature is attributed to the tribologically transformed structure (TTS) as discussed in Ref. [34].

### 3.2. Effect of testing conditions on wear damage

Fig. 8 presents the maximum wear depth measured from the samples tested under varying oscillation amplitudes. The observed trend indicates an increase in wear depth from the smallest amplitude of 2 mm to the medium amplitude of 5 mm. However, from the medium amplitude of 5 mm to the largest amplitude of 8 mm, the wear depth shows limited increases. This behaviour can be explained based on the theory of the existence of an upper threshold for the frictional energy density, which is determined by the sliding ratio. This threshold limits the maximum local wear that a specific point of the wear surface can accumulate per cycle, assuming the other parameters remain unchanged [11]. These findings indicate that the maximum frictional energy density is reached within the range of oscillation amplitudes between 2 and 5 mm. This limit on the local wear depth does not imply that the global wear damage remains constant under larger oscillation amplitudes. While the volume of wear damage may increase with larger amplitudes, the wear depth remains constant. Regarding the effect of grease, its presence seems not reduce the maximum wear; on the contrary, it slightly increases it. This effect can be attributed to the grease being squeezed out of the contact area during the early cycles of the test, subsequently serving only to prevent debris from being ejected. Consequently, this leads to a slight increase in wear damage, resulting in a worsened wear scenario in comparison with the unlubricated tests.

Fig. 9a shows the maximum wear depth under different contact forces and oscillation amplitudes. The observed trend shows that the wear depth increases with the contact force, but not linearly. These results suggest that under a higher load the maximum wear depth could reach a maximum limit value, which can be explained because of the transition towards partial slip where little wear damage occurs and fretting fatigue becomes the predominant damage mode [35,36]. From the wear maps shown in Fig. 9b, it can also be observed a reduction of the total sliding distance with the increase of the contact force for dry contact tests, where the sliding distance is estimated as 5.1 mm for a contact force of 10 kN, 3.9 mm for a contact force of 20 kN, and 3.5 mm for a contact force of 30 kN. This phenomenon can be also explained because of the transition towards partial slip, where fretting loops have a closed shape thus reducing the total sliding distance [36].

Fig. 10 shows the maximum wear depth under different oscillation frequencies. No clear influence can be observed under the range of frequencies tested in this study. Tests D12 and L12 conducted at 2 Hz are one of the cases where the greases lubricated test resulted in less wear damage. This may indicate that this particular grease performs better at higher speeds.

Fig. 11a presents the wear depth versus two contact geometry parameters: the ball diameter and contact conformity. Results show that with a larger ball and the same conformity of 0.52 it reduces the wear depth. A bigger ball and larger groove radius result in an increase in the contact area and a decrease in the contact pressure, which may explain the reduction of the wear depth. Increasing the conformity also reduces the wear depth. The explanation of this behaviour is less evident compared to the ball diameter. The condition is also tested when the conformity is increased by enlarging the groove radius and keeping the ball diameter unchanged. This results in higher contact pressure. However, the shape of the contact area changes, the major axis of the contact area becomes smaller, and the minor axis wider, which improves the distribution of the slip in the contact area, as also observed by Schwack et al. [17]. A comparison of wear maps of dry tests under different contact geometries is presented in Fig. 11b where the increase of the worn area occurs with a bigger ball and the decrease of the worn area is seen with higher conformity, but with a reduced ovalised shape.

The last parameter analysed from these experimental tests is the number of cycles. Fig. 12a shows a plot of the wear depth at two different numbers of cycles of 3000 and 10000, respectively. It can be observed that little damage has been accumulated during the first 3000 cycles. The reason for the small amount of wear during the earlier cycles might be due to the formation of a TTS layer. In a material that forms TTS, the frictional energy in early cycles is used to produce this layer, thus no wear is produced. Fig. 12a also shows an interesting observation regarding the effect of lubrication. It can be observed that at the first 3000 cycles, the wear depth in the grease lubricated test is not higher than that from the dry configuration. This might be because the grease has not been completely squeezed out of the contact. The positive effect of grease during the first cycles can be noticed in the comparison of the wear marks between the dry and lubricated conditions presented in Fig. 12b.

### 3.3. Coefficient of friction

The tangential force was measured during the tests and used to

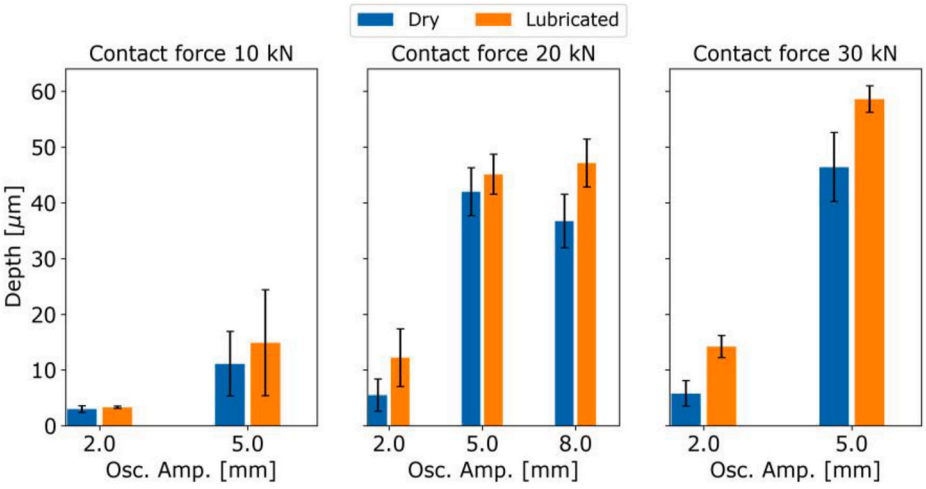


**Fig. 8.** Maximum wear depth under different oscillation amplitudes.

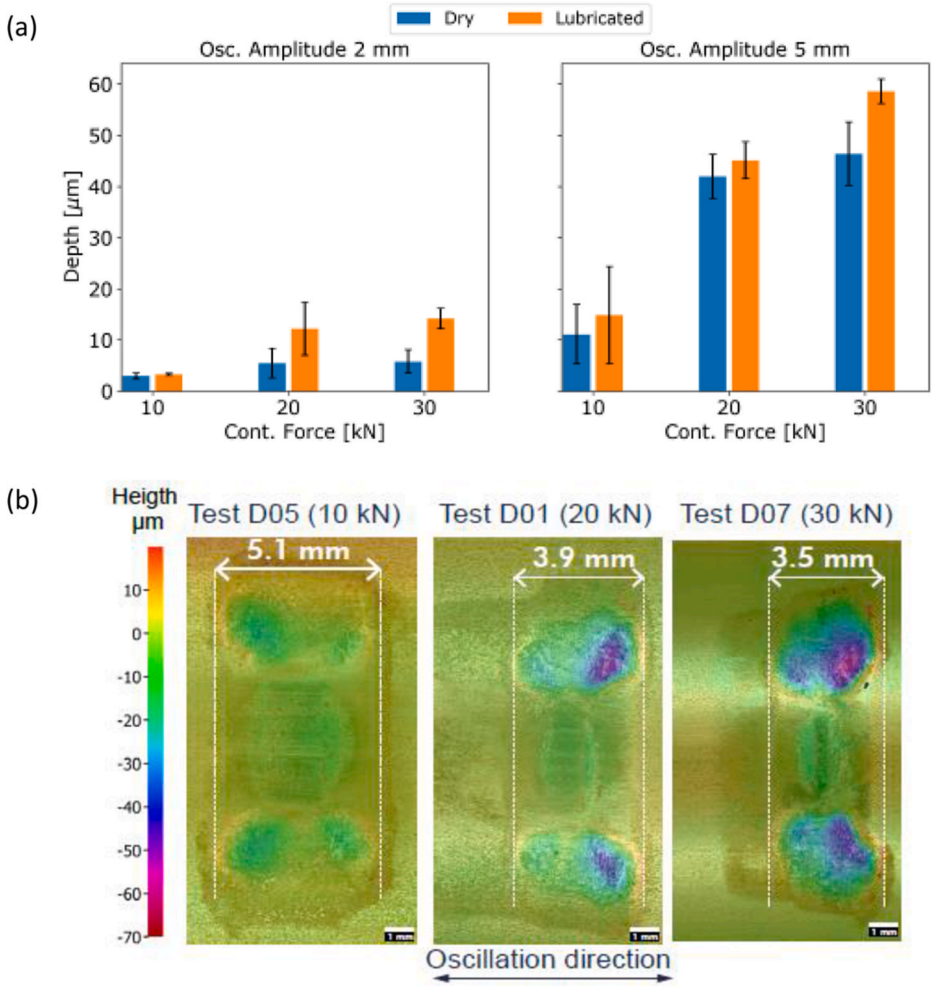


**Fig. 9.** Results under different contact forces and oscillation amplitudes: (a) Comparison of maximum wear depth and (b) Comparison of wear maps of dry tests.

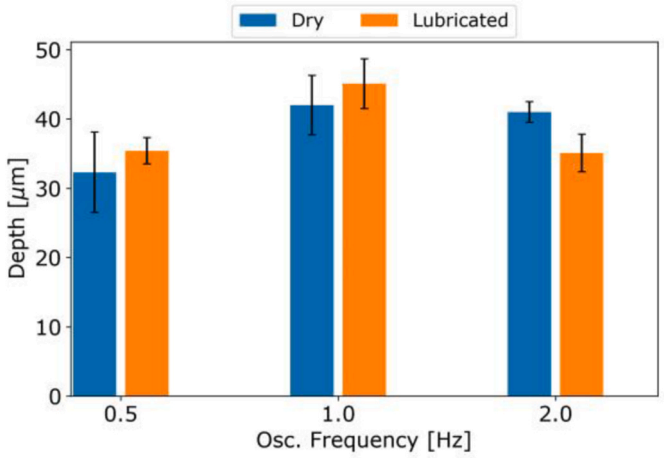


**Fig. 10.** Maximum wear depth under different oscillation frequencies.

estimate the coefficient of friction between the ball and the grooved surface of the tested samples. As the tests were conducted with the surface of the bottom sample without lubrication and the surface of the top sample lubricated, the results of the coefficient of friction presented in this section represent an average between both conditions. However, for lubricated conditions under small oscillations the grease is expected to be squeezed out of the contact area thus creating a similar behaviour to the dry contact due to starved lubrication condition. This is also confirmed by the minimal difference between the wear marks observed under dry and lubricated conditions, shown in Section 3.2.

Fig. 13a presents the time series of the estimated coefficient of friction for all test conditions, obtained by the ratio of the measured tangential force over the contact force, with exception of test 10 due to issues with the controller. A stable frictional behaviour is observed in all tests. Fig. 13b shows the average coefficient of friction as function of the oscillation amplitude under different levels of the contact force. The error bars represent the standard deviation due to the variation of the coefficient of friction over time. The average values range between 0.08 and 1.14; therefore, the coefficient of friction of 0.1 has been used in the FE wear modelling, presented in Section 2.5.

### 3.4. Frictional energy density distribution

The frictional energy density distribution is obtained by result post-processing from the FE models by using a script developed in Python capable to extract the contact pressure (CPRESS) and the sliding distance (CSLIPEQ) of every time step of the FE computation. From these data, the total energy density accumulated in one cycle is calculated as described in Equation (4) and stored in a new Field Output for graphical post-processing. Equation (4) is numerically equivalent to Equation (2).

$$E_{d,total} = \sum_{n=1}^{n=N} \mu P(n)(\Delta(n) - \Delta(n-1)) \tag{4}$$

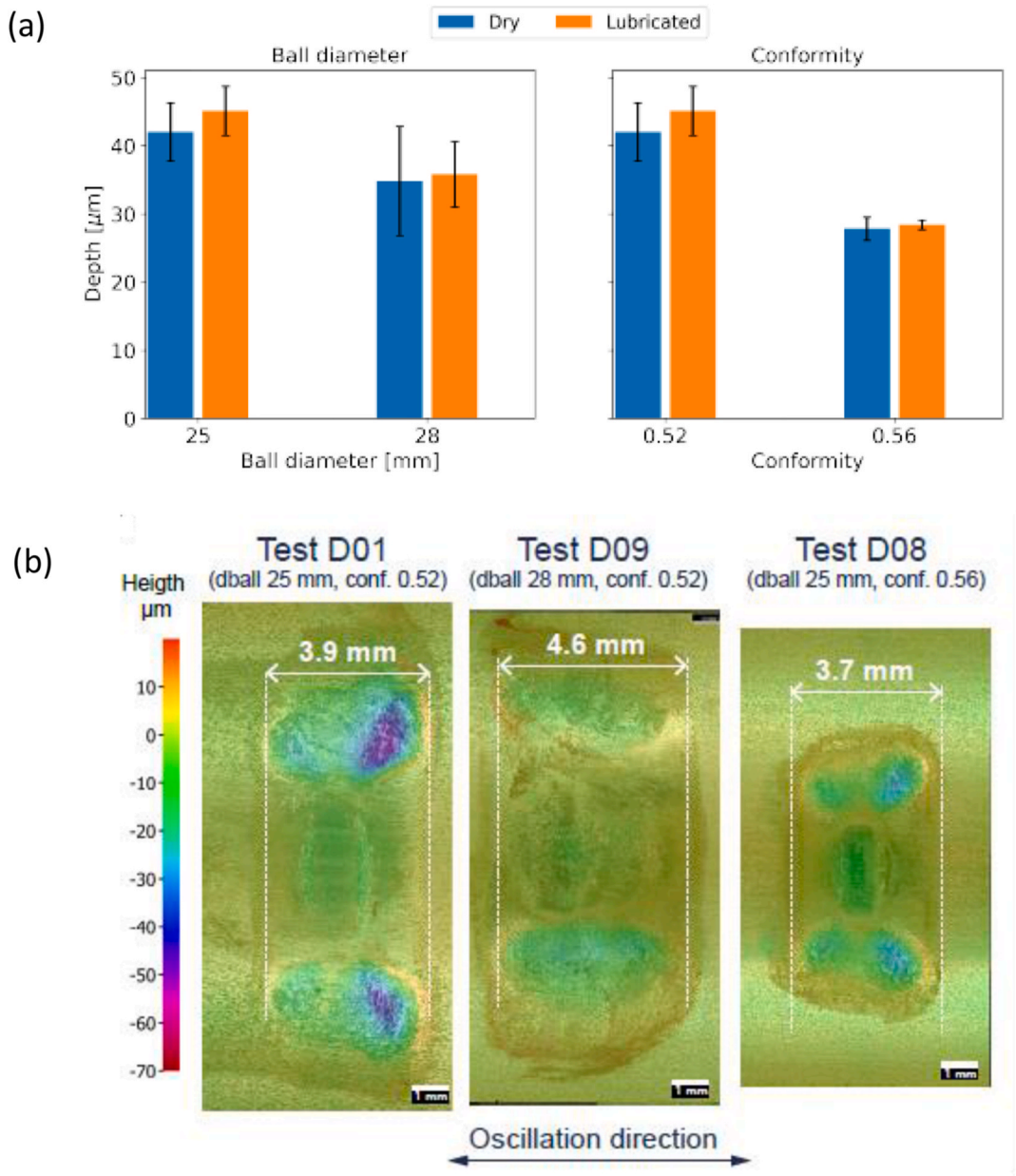


**Fig. 11.** Results for different contact geometries: (a) Comparison of maximum wear depth and (b) Comparison of wear maps of dry tests.

where $E_{d,total}$ is the total accumulated frictional energy density, $N$ is the total number of time increments in the oscillation cycle, $\mu$ is the coefficient of friction, and $P(n)$ and $\Delta(n)$ is the contact pressure (CPRESS) and sliding distance (CSLIPEQ) obtained from the FE model at the time increment $n$.

Fig. 14 shows the frictional energy density distribution post-processed from the FE modelling results compared to the respective worn surface scars from the experimental tests under different oscillation amplitudes, contact forces and contact geometries, respectively. The plots presented in Fig. 14 summarise the maximum frictional energy density obtained from each FE model plotted together with the maximum wear depth measured from the experimental tests. The comparison between the FE modelled frictional energy density distribution and the measured wear maps demonstrates a strong degree of correlation in nearly all cases, except for varying conformity cases of the contact geometry. Generally, both the FE modelled frictional energy density and the measured wear maps exhibit similar distributions, with the majority of frictional energy density and wear depth shows concentrations at the ends of the long axis of the contact area due to the occurrence of differential slips or Heathcote slips in highly conformal contacts between balls and grooved surfaces.

One notable difference observed between the energy density distribution from the FE models and the wear maps from the experimental tests is that the energy density from the FE models is equally distributed at both ends of the worn surfaces, while the experimentally measured wear depth is typically higher on one of the ends of the worn surface. This distinction may be explained by changes in the contact behaviour as the wear scar develops over cycles. Regarding the case with different conformity, it is expected that a higher conformity of the contact geometry leads to increased contact pressures, resulting in higher energy density. Schwack [17] argued that higher conformity also produced a change in the slip distribution, leading to lower frictional energy density. The fact that this is not observed in the developed FE model could be attributed to the different geometries used in the two studies. Regarding the assumptions made in the FE models that may impact the results, the most important one is that the frictional energy density is

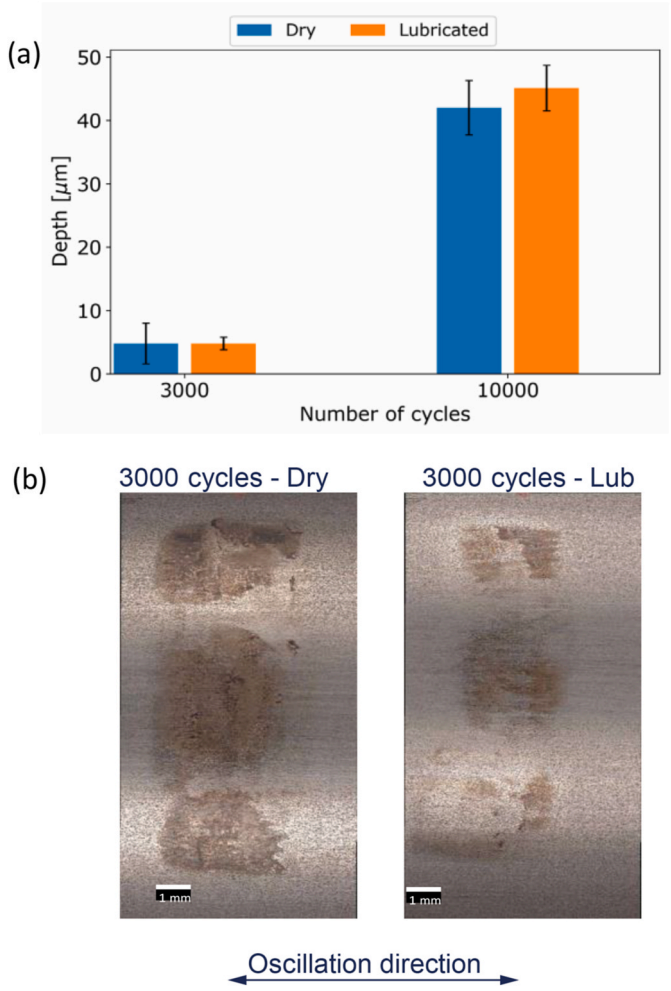


**Fig. 12.** Results for different number of cycles for dry and lubricated tests: (a) Comparison of maximum wear depth and (b) Comparison of wear maps.

simulated on unworn surface. As wear progresses, it would impact the contact pressure and the slip distribution. However, for a short test where the maximum wear depth is below 100 μm, it is assumed that the impact of this simplification is not sufficient enough affecting the modelling results.

The comparison between the maximum frictional energy density from the FE modelling and wear depth from the experimental measurement, as presented in Fig. 15, makes it possible to analyse whether the trends of the different testing parameters are similar to those observed in the experiments. This analysis confirms the similarity in trends for almost all the cases, with one notable exception being the model with different conformity. Another validation analysis conducted to confirm the frictional energy density as an indicator of fretting wear involves post-processing the evolution of this parameter along a path on the worn surface to obtain a distribution profile from the FE model, which is then compared to the wear profile measured from the experimental tests. Fig. 16 presents this comparison for the case with an oscillation amplitude of 5 mm and a contact force of 20 kN. The comparison reveals a strong similarity between the profiles of the FE modelled frictional energy density and the experimental measured wear depth, despite the frictional energy density results do not account for the changes caused by the wear scar. This correspondence further reinforces the validity of the frictional energy density as an indicative measure of fretting wear under the conditions investigated in this study.

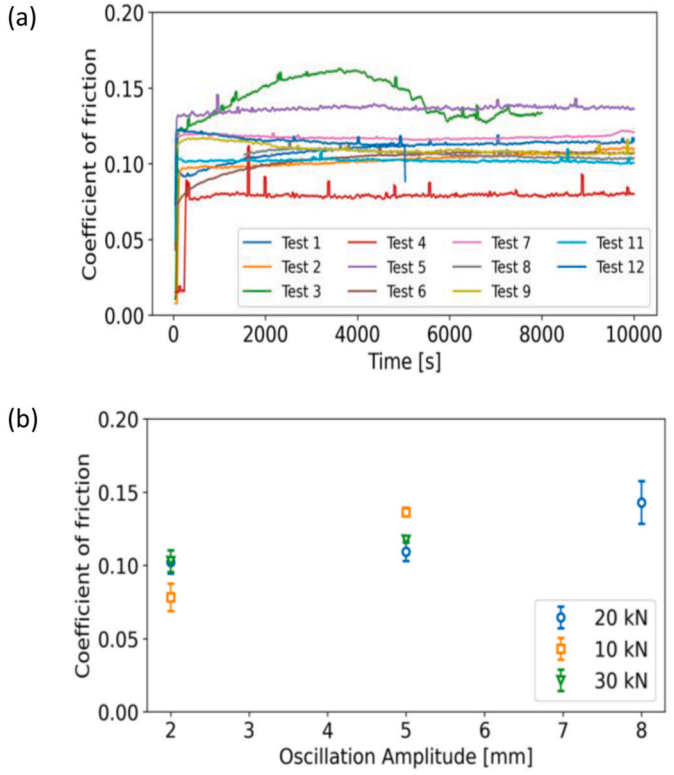


**Fig. 13.** Results of the measured coefficient of friction: a) Coefficient of friction for all tests versus time and b) Average coefficient of friction as function of the oscillation amplitude and contact force.

## 4. Discussion

The primary objective of this study is to investigate the impact of key parameters on fretting wear under WT pitch bearing operating conditions. The ultimate goal is to gain an improved understanding of this wear mode and based on the findings, to provide valuable research methods to predict and mitigate its occurrence. This objective is achieved by developing a simplified medium-scale experimental method that enables conducting tests under the actual pitch bearing operating conditions in an accelerated and inexpensive way.

### *4.1. Analysis of the studied parameters for control and mitigation of fretting wear*

The findings presented in this study provide the following recommendations to control key parameters to mitigate wear damage caused by small-amplitude oscillations in pitch bearings. These are valid for the specific test conditions investigated in this study, taking into account the limitations of the simplified test setup, as discussed in Section 4.2.

- **Oscillation amplitude:** The oscillation amplitude is directly related to the upper limit of the wear damage determined by the maximum frictional energy density that a surface point can accumulate in one oscillation. This suggests that one possible approach to mitigate the wear damage would be either to minimise the oscillating angle amplitude as much as possible below the transition to partial slip. Another possible approach is to pitch the blade at amplitudes larger than the critical angle $\theta_{crit}$ defined by Harris et al. [2] when a second ball overlaps the contact stress area and the lubrication is argued to work better. In other words, by controlling the number of oscillations whose amplitudes are between the amplitude that corresponds to a sliding ratio equal the limit for partial slip transition and the Harris' critical angle, the wear damage may be minimised.

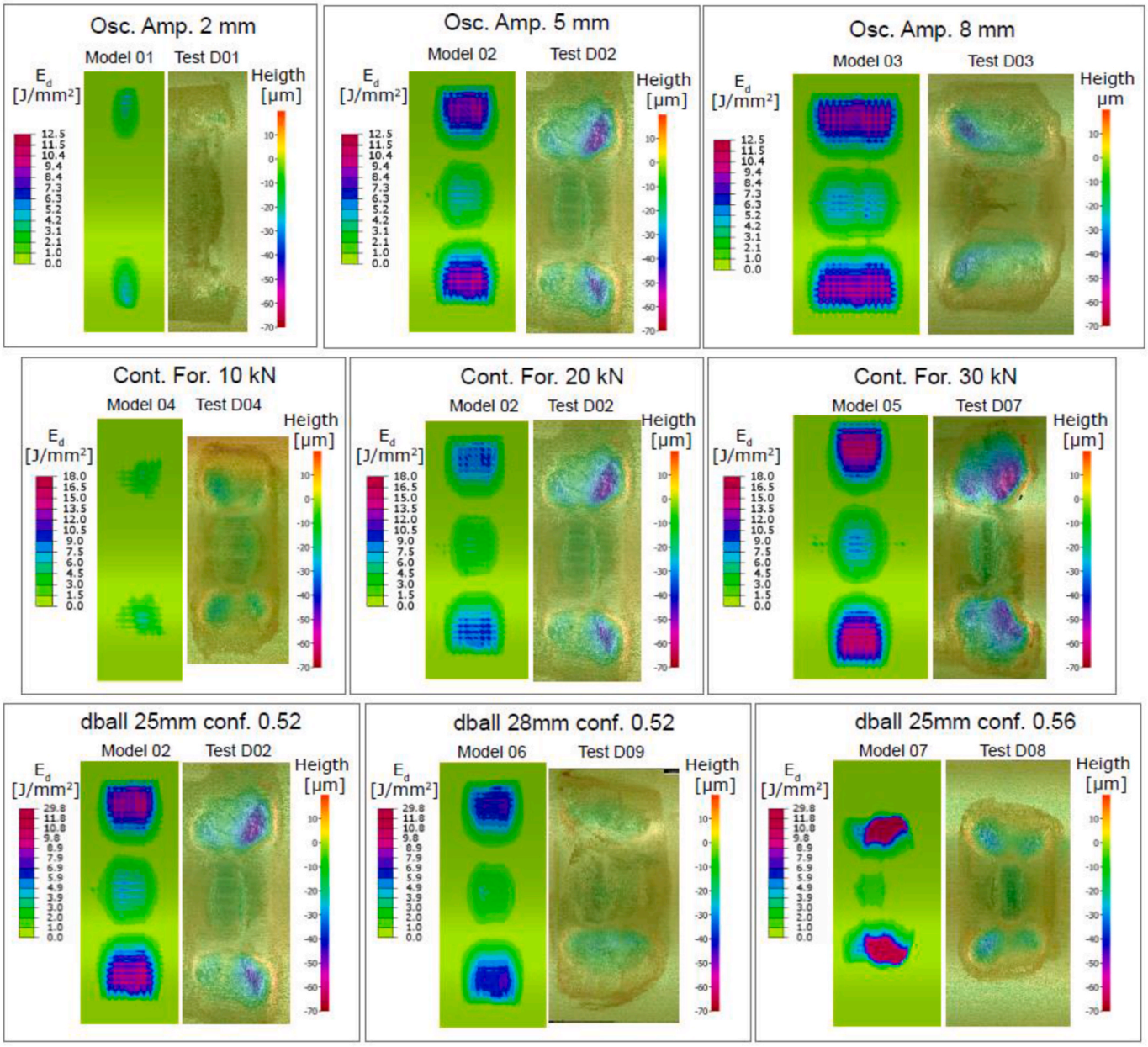


**Fig. 14.** Comparison between FE modelled frictional energy density and experimentally measured wear depth under the equivalent conditions. First row: varying oscillation amplitudes, second row: varying contact forces, third row: varying contact geometries.

- **Contact force:** Experimental results obtained in this study show an intuitive result of the effect of the contact force on the wear damage. The wear depth increases with the contact force. Therefore, to reduce the wear damage, from the contact force point of view, it is critical to control and reduce the load. Unfortunately, this cannot be achieved easily, as the loads acting on the pitch bearing depend on many variables and operating conditions. However, it is possible to improve the load distribution in the design phase of pitch bearings by modifying the flexibility of the hub, which in practical terms reduces the contact forces on the most loaded rolling elements of a pitch bearing [37].
- **Oscillation frequency and lubrication:** These two parameters do not show a significant effect on the wear damage. However, this study does not focus on analysing the effect of different greases on wear thus only one grease is used in the tests. A different grease could work better under pitch bearing operating conditions. The constant amplitude oscillations is probably one of the worst lubricated conditions for fretting wear, as it does not allow relubrication and lead to lubrication starvation [38]. A more in-depth analysis is required to identify the relevant grease properties that reduce wear under the most critical fretting wear condition, such as high loads and medium oscillation amplitude range. However, the detailed analysis of effect of grease properties on wear damage is not within the scope of this study.
- **Contact geometry:** The medium-scale test rig developed in this study allows the understanding of the effect of the contact geometry on wear, when the ball kinematics is representative of the motion of actual pitch bearings. The results show that either increasing the ball size or the conformity reduces the wear damage produced by small oscillations. Nevertheless, increasing the ball size could probably lead to a bearing with fewer rolling elements, and therefore an increase in the load on each ball. On the other hand, an increase in the conformity could result in a change in the bearing geometry and its stiffness, also increasing the maximum load of the rolling elements.

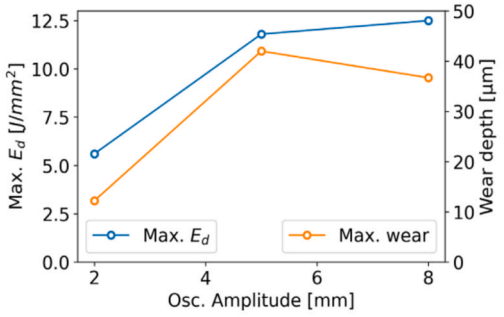


(a) Max. Ed and wear depth under different oscillation amplitudes

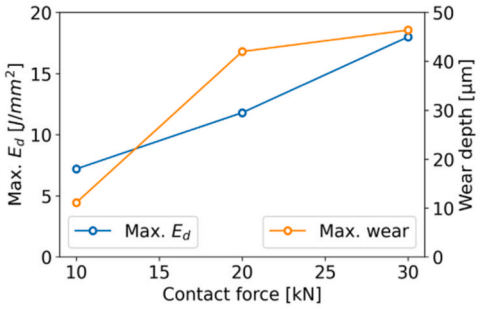


(b) Max. Ed and wear depth under different contact forces

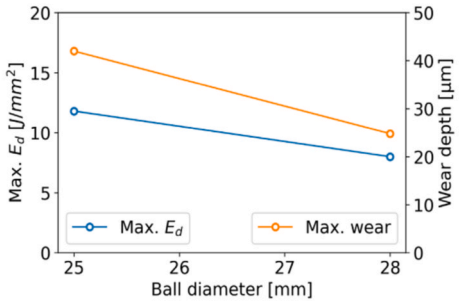


(c) Max. Ed and wear depth under different ball diameter

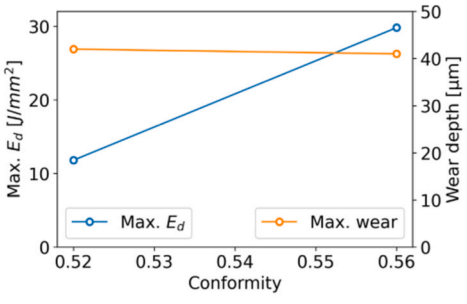


(d) Max. Ed and wear depth under different conformity values

**Fig. 15.** FE modelled maximum frictional energy density and experimental measured wear depth under different (a) oscillation amplitudes; (b) contact forces; (c) ball diameters and (d) conformity values.

Thus, even though modifications to the contact geometry have the potential to mitigate fretting wear, they must be analysed together with other factors to achieve an optimum design of a pitch bearing.

### 4.2. Limitations and potential of the developed methods

There are a number of limitations of the experimental method developed in this study. The first limitation is related to the material selection. Instead of using the commonly employed 42CrMo4 steel, the tool steel O1 is chosen for the test samples for reducing the cost of heat treatment. However, despite this difference, a verification has been conducted to ensure that the surface hardness, mechanical properties, and chemical composition of the tool steel O1 are within the same range as those of the bearing steel of pitch bearings. The different heat treatment method of through hardening has been applied to the test samples, it does not significantly impact the results of the wear tests. The same surface hardness ensures that the wear rate behaves similarly to that using the bearing steel, provided that the composition of the steel does not induce changes in the wear mechanism, considering that wear properties are not only dependent on surface hardness [33]. In this regard, the wear marks produced exhibit the same features as that of other similar fretting wear tests conducted at different scales for WT pitch bearings [17,39].

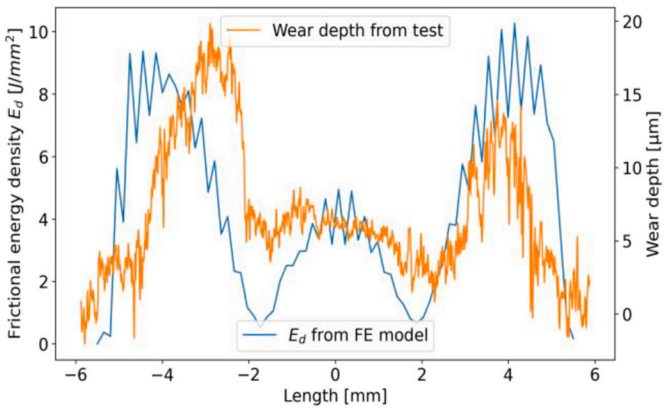


**Fig. 16.** FE modelled frictional energy density ($E_d$) compared to experimentally measured worn surface (height) under an oscillation amplitude of 5 mm.

The second limitation of this experimental study relates to the testing conditions, which have been designed to reproduce wear damage caused by small amplitude oscillations for pitch bearings. However, it is essential to acknowledge that these testing conditions represent simplified pitch bearing operating conditions. In actual WTs, pitch bearings operate under significantly more complex conditions, which include variable oscillation amplitude, frequency, and contact force. Furthermore, the current test setup does not account for the effect of the contact angle in most ball pitch bearings, which is another important factor influencing the wear behaviour of pitch bearings in actual operating conditions.

The final limitation of this experimental study is related to lubrication. The scope of the study is to analyse the effect of both dry and lubricated contacts but not the effect of grease properties on wear damage. However, it is essential to acknowledge that replicating the actual pitch bearing lubrication conditions in this simplified test setup is not feasible. There are two main reasons for this limitation. Firstly, the test setup does not account for the complex interactions between the grease and all the components in actual pitch bearings, such as multiple rolling elements and cages. Secondly, in WT pitch bearings, the raceways are sealed, which is not the case in the open contact geometry of the test condition adopted in this study. As a result, while this study provides valuable insights into the effect of dry and lubricated contacts under simplified conditions, it may be more conservative than needed for the lubricated tests. While the simplified setup allows for controlled and cost-effective testing, it may not fully capture the intricacies of the actual operational environment of pitch bearings, limiting the direct applicability of the findings to real WT systems. Therefore, it is crucial to consider these limitations when interpreting and extrapolating the results of this study to practical WT applications.

The FE model developed in this study provides a good method to estimate the occurrence of fretting wear based on the frictional energy density and shows a good correlation with the experimental results.

However, its application is limited due to two main factors. Firstly, the incapability of including the effect of lubrication. This can affect contact results such as the contact pressure and surface sliding, and also the frictional behaviour. Nevertheless, this FE modelling method can be useful for designing purposes of pitch bearings and to compare the effect of different variables as it has been demonstrated in this study. Another significant limitation of the developed FE model is that it only simulates a single oscillation cycle and does not consider the effect of accumulated wear damage over time. While this limitation has been addressed in various applications using the user-subroutine UMESHMOTION, such as in finger lock chucks of landing gears [40] or modular taper interfaces of hip implants [41]. However, this approach introduces additional constraints and drastically increases computational times without yielding substantial improvements in result accuracy thus it has not been adopted in this study.

## 5. Conclusions

This study focuses on investigating the wear damage caused by small-amplitude oscillations under simplified operating conditions of WT pitch bearings. The specially designed new test rig has enabled the replication of wear damage by conducting cost-efficient and accelerated experiment, taking into account test scale and ball kinematics effects similar to pitch bearing operations. The main conclusions are as follows.

- Wear marks show a wear pattern where greater wear and oxidation levels are located at the ends of the long axis of the elliptical contact area. This is where the maximum frictional energy density is accumulated most, mainly driven by the sliding distance;
- The wear damage reaches a limit in terms of the wear depth that can accumulate by the oscillation of one ball on a surface point, and this limit is primarily influenced by the oscillation amplitude;
- Wear damage increases with the increase of the contact force during the tests, equivalent to contact pressure in the range of 2.2 and 3.2 GPa;
- Oscillation frequency and lubrication do not exhibit a significant effect on wear damage under the range of tested parameters investigated in this study;
- The contact geometry has an important effect on wear damage. It has been found that wear damage can be reduced by increasing the ball diameter or enhancing the conformity between the contacting surfaces;
- The frictional energy density obtained from the FE models exhibits a strong correlation with the measured wear depth from the experimentally tested samples, with a potential to predict the occurrence of wear by employing the developed FE modelling method;
- Controlling oscillation amplitude and contact pressure of pitch bearings in WT operation can be effective ways to mitigate wear damage development. Future tests should focus on variable testing conditions and exploring lubrication effects.

## CRediT authorship contribution statement

**Eladio Hurtado Molina:** Writing – original draft, Visualization, Validation, Methodology, Investigation, Formal analysis. **Hui Long:** Writing – review & editing, Supervision, Methodology.

## Declaration of competing interest

The authors declare that they have no known competing financial interests or personal relationships that could have appeared to influence the work reported in this paper.

## Acknowledgments

The first author would like to acknowledge the financial support received from the Chilean National Agency for Research and Development (ANID)/Scholarship Program/Doctorado Becas Chile/2018–72190145.

## Data availability

Data will be made available on request.

## References

[1] M. Stammler, A. Reuter, Blade bearings : damage mechanisms and test strategies, in: *The 2nd Conference for Wind Power Drives*, WD, 2015, 03 2015.
[2] T. Harris, J.H. Rumbarger, C.P. Butterfield, Wind Turbine Design Guideline DG03: Yaw and Pitch Rolling Bearing Life, NREL, 2009, p. 63, no. December.
[3] A. Greco, S. Sheng, J. Keller, A. Erdemir, Material wear and fatigue in wind turbine Systems, Wear 302 (1–2) (2013) 1583–1591.
[4] D. Godfrey, Fretting corrosion or false brinelling? Tribol. Lubric. Technol. 59 (December) (2003) 28–30.
[5] C.L. Lin, K. Fallahnezhad, O. Brinji, P.A. Meehan, Mitigation of false brinelling in a roller bearing: a case study of four types of greases, Tribol. Lett. 70 (1) (2022) 1–18.
[6] K. Fallahnezhad, S. Liu, O. Brinji, M. Marker, P.A. Meehan, Monitoring and modelling of false brinelling for railway bearings, Wear 424–425 (2019) 151–164.
[7] M. Godet, The third-body approach: a mechanical view of wear, Wear 100 (1–3) (1984) 437–452.
[8] Y. Berthier, D. Play, Wear mechanisms in oscillating bearings, Wear 75 (1982) 369–387.
[9] Mineralogy: magnetite & hematite." https://lifeinplanelight.wordpress.com/2011/02/28/mineralogy-magnetite-hematite-minerals-of-the-week-2/. Accessed: 2022-03-18.
[10] J.A. Collins, Fretting-fatigue damage-factor determination, Journal of Manufacturing Science and Engineering, Transactions of the ASME 87 (3) (1965) 298–302.
[11] S. Fouvry, T. Liskiewicz, P. Kapsa, S. Hannel, E. Sauger, An energy description of wear mechanisms and its applications to oscillating sliding contacts, Wear 255 (aug 2003) 287–298.
[12] T. Maruyama, T. Saitoh, A. Yokouchi, Differences in mechanisms for fretting wear reduction between oil and grease lubrication, Tribol. Trans. 60 (3) (2017) 497–505.
[13] F. Schwack, N. Bader, J. Leckner, C. Demaille, G. Poll, A study of grease lubricants under wind turbine pitch bearing conditions, Wear 454–455 (2020) 203335.
[14] J.L. Mo, M.H. Zhu, J.F. Zheng, J. Luo, Z.R. Zhou, Study on rotational fretting wear of 7075 aluminium alloy, Tribol. Int. 43 (5–6) (2010) 912–917.
[15] R. Januszewski, V. Brizmer, A. Kadiric, Effect of lubricant properties and contact conditions on false brinelling damage, Tribol. Trans. 66 (2) (2023) 350–363.
[16] P. He, R. Hong, H. Wang, C. Lu, Pitch bearing/raceway fretting: influence of contact angle, Proc. IME C J. Mech. Eng. Sci. 233 (5) (2019) 1734–1749.
[17] F. Schwack, F. Prigge, G. Poll, Finite element simulation and experimental analysis of false brinelling and fretting corrosion, Tribol. Int. 126 (2018) 352–362.
[18] I. McColl, J. Ding, S. Leen, Finite element simulation and experimental validation of fretting wear, Wear 256 (11) (2004) 1114–1127.
[19] C. Mary, S. Fouvry, Numerical prediction of fretting contact durability using energy wear approach: optimisation of finite-element model, Wear 263 (sep 2007) 444–450.
[20] A. Daidié, Z. Chaib, A. Ghosn, 3D simplified finite elements analysis of load and contact angle in a slewing ball bearing, J. Mech. Des. 130 (2024) 082601.
[21] M. Graßmann, F. Schleich, M. Stammler, Validation of a finite-element model of a wind turbine blade bearing, Finite Elem. Anal. Des. 221 (2023) 103957.
[22] F. Schwack, M. Stammler, H. Flory, Free contact angles in pitch bearings and their impact on contact and stress conditions, in: Wind Europe Conference Paper, 2016, 2016 no. September.
[23] En19 datasheet. https://www.westyorkssteel.com/files/en19t.pdf. (Accessed 13 July 2022).
[24] O1 datasheet. https://www.westyorkssteel.com/files/o1.pdf. (Accessed 13 July 2022).
[25] Castrol UK Limited, Product Data LMX Grease, 2002.
[26] J. Hintikka, A. Mäntylä, J. Vaara, T. Frondelius, A. Lehtovaara, Stable and unstable friction in fretting contacts, Tribol. Int. 131 (July 2018) (2019) 73–82.
[27] S.R. Pearson, P.H. Shipway, Is the wear coefficient dependent upon slip amplitude in fretting? Vingsbo and Söderberg revisited, Wear 330–331 (2015) 93–102.
[28] A. Sevinc, M. Rosemeier, M. Bätge, R. Braun, F. Meng, M. Shan, D. Horte, C. Balzani, A. Reuter, IWES Wind Turbine IWT-7.5-164, 2014, p. 62, no. June.
[29] H.L. Heathcote, The ball bearing: in the making, under test and on service, Proceedings of the Institution of Automobile Engineers 15 (1) (1920) 569–702.
[30] Y. Berthier, L. Vincent, M. Godet, Velocity accommodation in fretting, Wear 125 (1–2) (1988) 25–38.
[31] T.A. Harris, Advanced Concepts of Bearing Technology: Rolling Bearing Analysis, fifth ed., CRC Press, Boca Raton, 2006, 5th edition ed.
[32] K. Johnson, A review of the theory of rolling contact stresses, Wear 9 (1) (1966) 4–19.
[33] L. Bourithis, G. Papadimitriou, J. Sideris, Comparison of wear properties of tool steels aisi d2 and o1 with the same hardness, Tribol. Int. 39 (6) (2006) 479–489.

[34] E. Sauger, S. Fouvry, L. Ponsonnet, P. Kapsa, J.M. Martin, L. Vincent, Tribologically transformed structure in fretting, Wear 245 (1–2) (2000) 39–52.
[35] O. Vingsbo, S. Söderberg, On fretting maps, Wear 126 (2) (1988) 131–147.
[36] Z.R. Zhou, L. Vincent, Mixed fretting regime, Wear 181–183 (PART 2) (1995) 531–536.
[37] E. Hurtado, H. Long, J. Carrell, R. Dwyer-Joyce, W. Song, Effect of supporting structure flexibility on the load distribution of a wind turbine pitch bearing. 16th EAWE PhD Seminar on Wind Energy, 2020, pp. 183–190.
[38] S. Wandel, N. Bader, F. Schwack, J. Glodowski, B. Lehnhardt, G. Poll, Starvation and relubrication mechanisms in grease lubricated oscillating bearings, Tribol. Int. 165 (2022) 107276.
[39] F. Schwack, F. Halmos, M. Stammler, G. Poll, S. Glavatskih, Wear in wind turbine pitch bearings—a comparative design study, Wind Energy 25 (4) (2022) 700–718.
[40] M. Zhang, R. Jiang, H. Nie, A numerical study on the friction and wear predictions of finger lock chuck in landing gear, Proc. Inst. Mech. Eng. G J. Aerosp. Eng. 231 (1) (2017) 109–123.
[41] T. Bitter, I. Khan, T. Marriott, E. Lovelady, N. Verdonschot, D. Janssen, Finite element wear prediction using adaptive meshing at the modular taper interface of hip implants, J. Mech. Behav. Biomed. Mater. 77 (2018) 616–623.